Acta Cryst. (1971). A27, 97

Clustering in Fe–3.9 at. % Mo

BY T. ERICSSON*
AB Atomenergi, Box 43041, Stockholm 43, Sweden

J. B. COHEN
Department of Materials Science, The Technological Institute, Northwestern University, Evanston, Illinois, U.S.A.

(*Received* 2 *February* 1970 *and in revised form* 20 *April* 1970)

The diffuse X-ray scattering from a single crystal of Fe–3·9 at. % Mo has been measured at room temperature. A volume in reciprocal space was explored, which was chosen so that the intensity due to local order could be separated from the effects of different atomic sizes of the species and first-order thermal diffuse scattering making use of the symmetry of these contributions according to a theory by Borie & Sparks. The Warren local order parameters have been derived and used in a computer program to generate the corresponding atomic distributions. The Mo atoms formed clusters on the average 7 to 8 Mo atoms in size, the clustered regions having about twice the Mo concentration as the average alloy composition. The largest clusters contained about 40 Mo atoms. The shapes of all these regions were irregular. An analysis of the scattering due solely to the differences in atomic size of Fe and Mo indicates that the Fe atoms are displaced from lattice points by about 0·001 Å.

1. Introduction

Iron-rich Fe–Mo alloys form body-centred cubic (b.c.c.) solid solutions with a maximum Mo content of about 26 at.% at about 1400 °C (Hansen, 1958). Upon cooling a supersaturated solid solution decomposes, as the low temperature solubility is about 2 at.%. Employing electron microscopy, Hornbogen (1961) found that after annealing a 20 at.% Mo alloy at 500 °C for up to 500 hr, Mo-rich disks are found on dislocation loops lying in {100} planes. After 500 hr the disks convert to particles of a Mo-rich b.c.c. solid solution. The particles are stable at or below 500 °C but above 500 °C they convert into the phase Fe_3Mo_2. To explain the occurrence of the Mo-rich b.c.c. particles Hornbogen (1966) assumed the existence of a metastable miscibility gap. Marcus, Fine & Schwartz (1967) did not observe any Mo-rich disks in an Fe–6 at.% Mo alloy after annealing between 500 and 650 °C for various times. Instead, precipitation of Fe_2Mo started after about 100 hr in agreement with a recent determination of the Fe–Mo equilibrium diagram by Sinha, Buckley & Hume-Rothery (1967). However, from Mössbauer measurements Marcus, Fine & Schwartz (1967) found a tendency for Mo atoms to be surrounded by other Mo atoms in specimens annealed for only a few hours at 550 °C, long before the Fe_2Mo phase appeared.

Thus there is some evidence for clustering of Mo atoms being the first stage of the decomposition of Fe-rich Fe–Mo solid solutions. The present work aims at giving a detailed picture of the atomic configurations in the solid solution at an aging time below that at which the equilibrium phase separates from measurements of diffuse X-ray scattering. Sparks & Borie (1966) have suggested that it is possible to separate from the total diffuse scattering at only one temperature, the part which is due to local order, because of the symmetry of the contributing terms. (Here the term local order will be used in a general sense including clustering as well as short-range order).

This paper is the first 3-D test of this method, and we show that it allows quantitative study of the diffuse scattering from systems which cluster, as well as those with short-range order; previous to this development only the latter state could be studied in detail. Knowing the intensity due to local order, the Warren local-order parameters were derived, from which the atomic distributions were generated using a computer technique developed by Gehlen & Cohen (1965). The distributions found for this alloy showed clusters of about 7 to 8 Mo atoms with a maximum size of 40 atoms.

The separated scattering due to size differences of the atoms yielded information about the static displacements of Fe atoms from lattice points.

2. Diffraction theory

2·1. *General*

The coherently scattered intensity from a binary alloy can be written as the sum of the intensity associated with the Bragg peaks, I_{fund}, and the total diffuse intensity, I_D. Furthermore, I_D can be written as the sum of three terms

$$I_D=(I^0_{\text{SRO}}+I^0_{\text{SM}}+I^0_{H,\text{TDS}})Nx_Ax_B(f_A-f_B)^2 \qquad (1)$$

where I^0_{SRO} is the scattering due to local order, I^0_{SM} is the so-called size effect-modulation term and $I^0_{H,\text{TDS}}$ is due to first-order thermal diffuse and Huang (size) scattering. Each term can be written in electron units

* Present address: AB Volvo, Avd. 6630, Göteborg, Sweden.

as a series, correct to terms involving the squares of displacements of atoms from lattice points (Sparks & Borie, 1966; Borie & Sparks, 1971):

$$I^0_{\mathrm{SRO}} = \sum_l \sum_m \sum_n \alpha_{lmn} \cos 2\pi(h_1 l + h_2 m + h_3 n)\,, \quad (2)$$

$$I^0_{\mathrm{SM}} = -\sum_l \sum_m \sum_n (h_1 \gamma^x_{lmn} + h_2 \gamma^y_{lmn} + h_3 \gamma^z_{lmn}) \sin 2\pi(h_1 l + h_2 m + h_3 n)\,, \quad (3)$$

$$I^0_{\mathrm{H,TDS}} = \sum_l \sum_m \sum_n (h_1^2 \delta^x_{lmn} + h_2^2 \delta^y_{lmn} + h_3^2 \delta^z_{lmn} + h_1 h_2 \varepsilon^{xy}_{lmn} + h_2 h_3 \varepsilon^{yz}_{lmn} + h_3 h_1 \varepsilon^{zx}_{lmn}) \cos 2\pi(h_1 l + h_2 m + h_3 n)\,, \quad (4)$$

N is the number of atoms, x_A and x_B are the atomic fractions of elements A and B, f_A and f_B are scattering factors, l, m, n are atomic coordinates and h_1, h_2, h_3 are continuous variables in reciprocal space.*

$$\alpha_{lmn} = 1 - P^{AB}_{lmn}/X_B\,, \quad (5)$$

$$\gamma^x_{lmn} = 2\pi[F^{AA}_{lmn}\langle x^{AA}_{lmn}\rangle + F^{BB}_{lmn}\langle x^{BB}_{lmn}\rangle + F^{AB}_{lmn}\langle x^{AB}_{lmn}\rangle]\,, \quad (6)$$

$$\delta^x_{lmn} = (-2\pi^2)[F^{AA}_{lmn}\langle (x^{AA}_{lmn})^2\rangle + F^{BB}_{lmn}\langle (x^{BB}_{lmn})^2\rangle + F^{AB}_{lmn}\langle (x^{AB}_{lmn})^2\rangle]\,, \quad (7)$$

$$\varepsilon^{yz}_{lmn} = (-4\pi^2)[F^{AA}_{lmn}\langle y^{AA}_{mn} z^{AA}_{lmn}\rangle + F^{BB}_{lmn}\langle y^{BB}_{lmn} z^{BB}_{lmn}\rangle + F^{AB}_{lmn}\langle y^{AB}_{lmn} z^{AB}_{lmn}\rangle]\,. \quad (8)$$

The definitions of γ^y_{lmn}, γ^z_{lmn}, δ^y_{lmn}, δ^z_{lmn}, ε^{xy}_{lmn} and ε^{zx}_{lmn} are analogous. x^{ij}_{lmn}, y^{ij}_{lmn} and z^{ij}_{lmn} are the coordinates in the real lattice of the difference, $\bar{\delta}^{ij}_{lmn}$, of the deviations of an i atom and a j atom from their average positions. P^{AB}_{lmn} is the probability of finding a B atom next to an A atom for the vector (l,m,n). The quantities F^{AA}_{lmn} *etc.* are defined by

$$F^{AA}_{lmn} = [f_A/(f_A - f_B)]^2(x_A/x_B + \alpha_{lmn})\,, \quad (9)$$

$$F^{BB}_{lmn} = [f_B/(f_A - f_B)]^2(x_B/x_A + \alpha_{lmn})\,, \quad (10)$$

$$F^{AB}_{lmn} = 2f_A f_B/(f_A - f_B)^2(1 - \alpha_{lmn})\,. \quad (11)$$

The averages $\langle x^{AA}_{lmn}\rangle$, *etc.* of the components of the deviations in interatomic spacings of two A atoms are to be taken over all i-j pairs separated by a constant $(\bar{r}_m - \bar{r}_n)$.

Inserting equations (2)–(4) into equation (1)

$$I_D(h_1,h_2,h_3) = \mathrm{N}x_A x_B(f_A - f_B)^2[I^0_{\mathrm{SRO}} + \mathrm{h}_1 Q_x(h_1,h_2,h_3) + h_2 Q_y(h_1,h_2,h_3) + h_3 Q_z(h_1,h_2,h_3) + h_1^2 R_x(h_1,h_2,h_3) + h_2^2 R_y(h_1,h_2,h_3) + h_3^2 R_z(h_1,h_2,h_3) + h_1 h_2 S_{xy}(h_1,h_2,h_3) + h_2 h_3 S_{yz}(h_1,h_2,h_3) + h_3 h_1 S_{zx}(h_1,h_2,h_3)]\,, \quad (12)$$

where

$$Q_x = -\sum_l \sum_m \sum_n \gamma^x_{lmn} \sin 2\pi(h_1 l + h_2 m + h_3 n)\,, \quad (13)$$

$$R_x = \sum_l \sum_m \sum_n \delta^x_{lmn} \cos 2\pi(h_1 l + h_2 m + h_3 n)\,, \quad (14)$$

$$S_{yz} = \sum_l \sum_m \sum_n \varepsilon^{yz}_{lmn} \cos 2\pi(h_1 l + h_2 m + h_3 n)\,. \quad (15)$$

The average atomic displacement for our case, a cubic crystal, must display symmetry across {100} and {110} planes and the same symmetry should exist in reciprocal space. From this symmetry the following relations have been derived by Sparks & Borie (1966) and Borie & Sparks (1971):

$$Q_y(h_1,h_2,h_3) = Q_x(h_2,h_1,h_3)\,, \quad (16)$$

$$Q_z(h_1,h_2,h_3) = Q_x(h_3,h_2,h_1)\,, \quad (17)$$

$$R_y(h_1,h_2,h_3) = R_x(h_2,h_1,h_3)\,, \quad (18)$$

$$R_z(h_1,h_2,h_3) = R_x(h_3,h_2,h_1)\,, \quad (19)$$

$$S_{xy}(h_1,h_2,h_3) = S_{yz}(h_3,h_2,h_1)\,, \quad (20)$$

$$S_{zx}(h_1,h_2,h_3) = S_{yz}(h_2,h_1,h_3)\,. \quad (21)$$

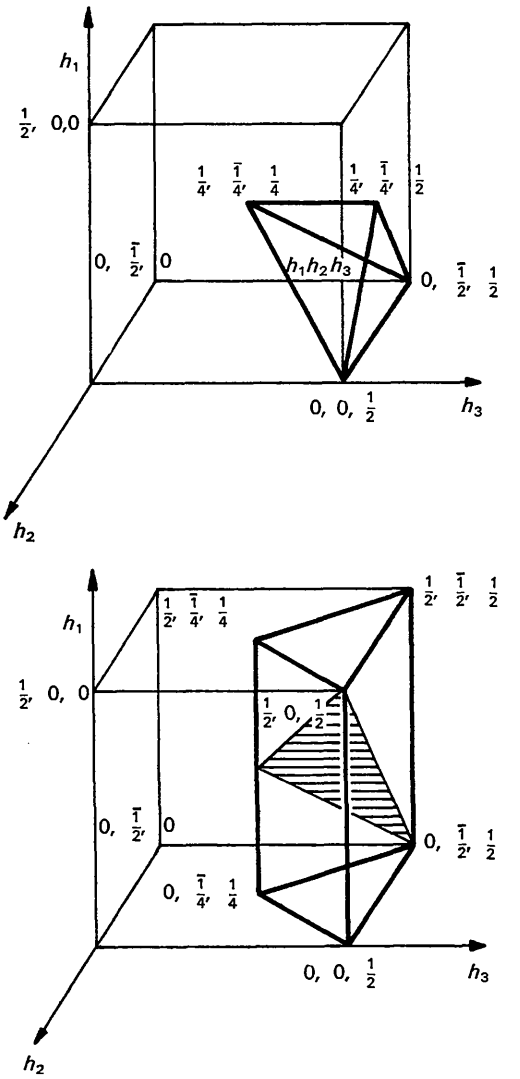

Fig. 1. Minimum repeat volumes for (*a*) I^0_{SRO} and (*b*) Q_x, R_x and S_{yz}.

* Defined so that l, m and n are integers and the fundamental peaks (101), (2$\bar{1}$1) *etc.* are labelled $(\frac{1}{2},0,\frac{1}{2})$, $(1,\frac{\bar{1}}{2},\frac{1}{2})$ *etc.*

Inserting these equations into equation (12) yields

$$I_D(h_1,h_2,h_3)=Nx_Ax_B(f_A-f_B)^2[I^0_{\mathrm{SRO}}(h_1,h_2,h_3)+h_1Q_x(h_1,h_2,h_3)+h_2Q_x(h_2,h_1,h_3)+h_3Q_x(h_3,h_2,h_1)+h_1^2R_x(h_1,h_2,h_3)+h_2^2R_x(h_2,h_1,h_3)+h_3^2R_x(h_3,h_2,h_1)+h_1h_2S_{yz}(h_3,h_2,h_1)+h_2h_3S_{yz}(h_1,h_2,h_3)+h_3h_1S_{yz}(h_2,h_1,h_3)]\,. \quad (22)$$

The expressions for γ, δ and ε contain the quantities $[f_A/(f_A-f_B)]^2$, $[f_B/(f_A-f_B)]^2$ and $f_Af_B/(f_A-f_B)^2$. They depend on $\sin\theta/\lambda$ but for a limited 2θ range they can be considered constants. (This dependence can be corrected for; see Appendix II.) Then not only I^0_{SRO} but also Q, R and S are true Fourier series in h_1, h_2 and h_3 with period 1. Using this periodicity it is possible to separate the various terms in equation (12) from each other (Sparks & Borie, 1966).

$$[I_D(h_1,h_2,h_3)-I_D(h_1-1,h_2,h_3)]/Nx_Ax_B(f_A-f_B)^2=\Delta_1I_D(h_1,h_2,h_3)=Q_x(h_1,h_2,h_3)+(2h_1-1)R_x(h_1,h_2,h_3)+h_2S_{yz}(h_3,h_2,h_1)+h_3S_{yz}(h_2,h_3,h_1)\,, \quad (23)$$

$$[I_D(h_1+1,h_2,h_3)-2I_D(h_1,h_2,h_3)+I_D(h_1-1,h_2,h_3)]/Nx_Ax_B(f_A-f_B)^2=\Delta_1^2I_D(h_1,h_2,h_3)=2R_x(h_1,h_2,h_3)\,, \quad (24)$$

$$[(I_D(h_1,h_2,h_3)-I_D(h_1-1,h_2,h_3))-(I_D(h_1,h_2-1,h_3)-I_D(h_1-1,h_2-1,h_3))]/Nx_Ax_B(f_A-f_B)^2=\Delta_1\Delta_2I_D(h_1,h_2,h_3)=S_{yz}(h_3,h_2,h_1)\,. \quad (25)$$

When I_D and the differences Δ_1I_D, $\Delta_1^2I_D$ and $\Delta_1\Delta_2I_D$ are known, then Q_x, R_x and S_{yz} and thus I^0_{SRO}, I_{SM} and $I_{H,\mathrm{TDS}}$ can be recovered from measurements at only one temperature. This requires measurements in volumes (h_1,h_2,h_3), (h_1-1,h_2,h_3) *etc.*

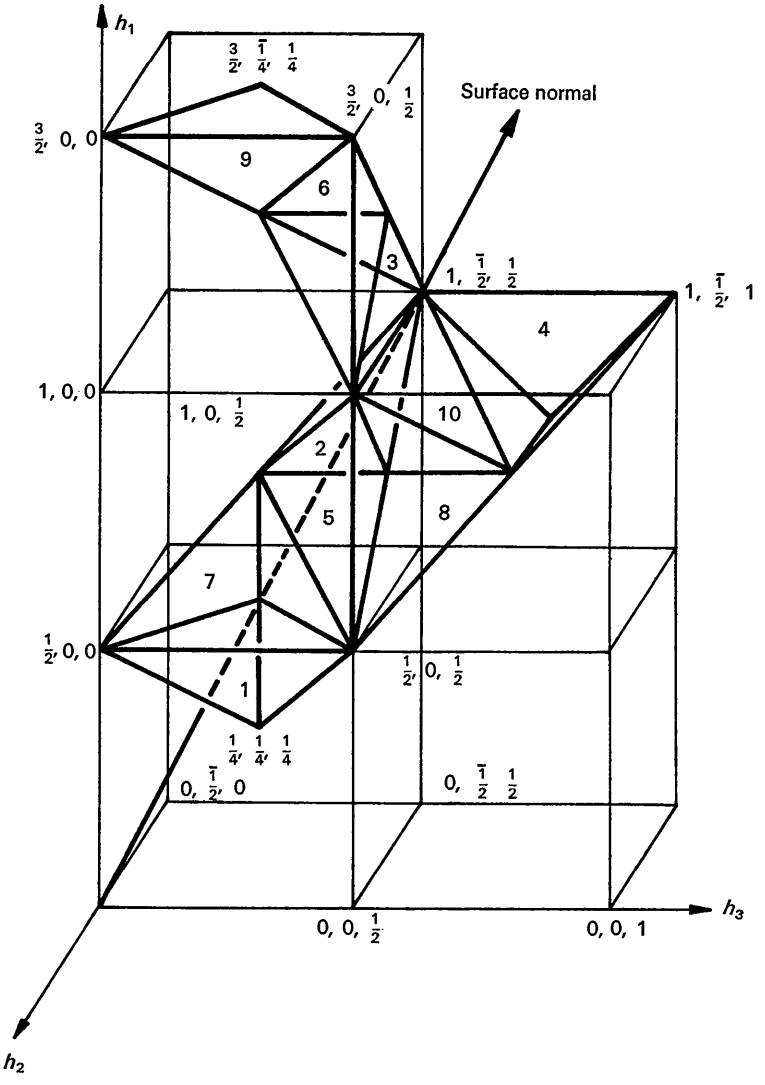

Fig. 2. Total explored volume in reciprocal space. The unit cell employed is half the usual one so that the (101) peak is labelled $(\frac{1}{2},0,\frac{1}{2})$ *etc.*

Because of cubic symmetry the minimum repeat volumes of I^0_{SRO}, Q_x, R_x and S_{yz} are much smaller than the unit cell in reciprocal space. For the b.c.c. lattice these volumes are shown in Fig. 1(*a*) and 1(*b*). For I^0_{SRO} it is a tetrahedron and for Q_x, R_x S_{xy} the part of a prism above or below the shaded plane in Fig. 1(*b*). This result for I^0_{SRO} and Q_x can be found in Sparks & Borie (1966) and for Q_x it is also developed in Appendix III.

2·2. *Application to the present problem*

The several volumes required, (h_1,h_2,h_3) *etc.*, can be condensed to a variety of small complex shapes, depending on the experiment. In Appendix I this is shown for the present problem, a b.c.c. crystal explored with a radiation of fairly long wavelength. (Co $K\alpha$ was employed to minimize fluorescence in this experiment). The final reciprocal lattice volume to be explored consists of ten tetrahedra like the one in Fig. 1(*a*), each one with a corner at a Bragg peak; see Fig. 2. The diffuse intensity was measured at 983 points in this volume. The experimental conditions did not permit higher angles than 136° 2θ with Co $K\alpha$; therefore Mo $K\alpha$ radiation was used for 89 points with high 2θ values.

The scattering factors, f_{Fe} and f_{Mo}, were taken from Batterman, Chipman & de Marco (1961) and from Cromer & Waber (1965) respectively, and the dispersion corrections for Co $K\alpha$ radiation from the tabulation by Cooper (1963) and for Mo $K\alpha$ radiation from *International Tables for X-ray Crystallography* (1962).

3. Experimental procedure

3·1. *Sample preparation*

A single crystal, nominally Fe–3·9 at.% Mo, 16 mm in diameter and 60 mm long, was given to us by P. Kettunen (Kettunen & Forstén, 1964). A disk was cut from the bar with its flat surfaces approximately parallel to a $(2\bar{1}1)$ plane. Analysis by X-ray fluorescence and with a microprobe indicated a uniform composition of $3{\cdot}86 \pm 0{\cdot}09$ at.% Mo.

After etching the specimen was annealed at 1050 °C for 1 hr (in an evacuated quartz capsule), water quenched, reannealed in a vacuum furnace at 550 °C for 5 hr and cooled at about 1·5 °C per sec. After final electropolishing the intensity of Fe $K\alpha$ fluorescence produced with Cu radiation was constant for 2θ larger than 20°, so no correction of the scattered intensity for roughness was needed in the region explored (de Wolff, 1956).

3·2. *Measurements*

Measurements were made with a General Electric XRD-5 diffractometer equipped with Picker electronics, a scintillation counter, and a pulse-height analyzer. The Co $K\alpha$ or Mo $K\alpha$ radiation employed was monochromated with a doubly bent LiF crystal as described by Schwartz, Morrison & Cohen (1963). The specimen was mounted in a vacuum camera (designed by Gragg, 1970), consisting of a beryllium hemisphere 100 mm in diameter pressed against a circular steel frame. This frame attached to the standard General Electric quarter-circle eucentric goniometer. The specimen was fastened on a smaller goniometer inside the camera, which permitted fine adjustments of its orientation. The initial orientation was $\chi = 90°$, with the $(2\bar{1}1)$ direction parallel to the φ rotation axis.

For Co $K\alpha$ a vanadium oxide filter with 90% transparency was inserted near the exit slits of the monochromator housing. The measured Co radiation was then counted for 220,000 counts of V $K\alpha$ fluorescence in a monitor counter. This procedure eliminated any variation in the beam power during the measurements. The background (0·22 cps) was measured with a lead beam trap in the sample position.

$\lambda/2$ and $\lambda/3$ contributions caused Fe fluorescence from the specimen which was accounted for as follows. The scattered intensity was measured with and without a MnO filter in front of the receiving scatter slit at many points. The transmission (T_{Co}) of the MnO filter for Co $K\alpha$ was determined by moving the filter in and out of a diffracted beam from a polycrystalline Si sample. The transmission (T_{Fe}) of the filter for Fe $K\alpha$ was measured by moving the filter in and out of the Fe fluorescence from the crystal produced by Cu $K\alpha$.

The observed intensities from the Fe–Mo crystal with the filter I_{MnO}, and without the filter, I, are related by

$$I[(1-x)T_{Co}+xT_{Fe}]=I_{MnO}\,, \qquad (26)$$

where x is the fraction of Fe $K\alpha$ radiation. The calculated intensity of Fe $K\alpha$ ($x\,.\,I$) varied less than 10% when I varied 500%. Its value was about 40% of the smallest intensity observed for any point, but more typically was 25%.

The direct beam intensity I_0 was measured with a polystyrene sample at 127° 2θ with a wide open scatter slit. The method has been described by Sparks & Borie (1966), the only differences being that we took the intensity in electron units per molecule of C_8H_8 (Compton + coherent) as 64·6 (calculated by Sparks & Borie, 1966) instead of their measured value of 61·1 because we felt that a number of important details may have been neglected in their measurement. Applying a 5% correction for double Bragg scattering (Warren & Mozzi, 1966; Strong & Kaplow, 1967), the intensity was $0{\cdot}53 \times 10^8 \pm 0{\cdot}08 \times 10^8$ cps.* After correction for background and fluorescence, the measured intensity from the Fe–Mo crystal was transformed into electron units per atom, I_{eu}/N,

* The error is due to uncertainties in slit dimensions and distance from the slits to the sample. Note however that in the conversion to I_{eu}/N, equation (27), I_0 is not used, but rather the counts from polystyrene. The error in I_0 due to uncertainties does not propagate to I_{eu}/N.

$$\frac{I_{eu}}{N} = \frac{I \times \text{atomic weight of alloy} \times (\mu/\varrho)p'}{I' \times \text{molecular weight of } C_8H_8 \times (\mu/\varrho)p} \times \left(\frac{I_{eu}}{M}\right)' \times \frac{1}{0{\cdot}95}. \quad (27)$$

$(I_{eu}/M)'$ is the calculated scattering per molecule from C_8H_8, I and I' are the measured intensities from the specimen and from C_8H_8 respectively, p and p' the polarization factors for the sample and C_8H_8 respectively, and 0·95 is the double Bragg scattering correction. The mass absorption coefficient for the sample $(\mu/\varrho)=69{\cdot}2$ was taken from Heinrich (1966) and for C_8H_8, $(\mu/\varrho)'=6{\cdot}2$, from *International Tables for X-ray Crystallography* (1962) adjusted by comparison with the measurements by Sparks & Borie (1966) for Cu $K\alpha$.

Finally, the Compton scattering from the alloy taken from *International Tables*, was subtracted from I_{eu}/N to get the total coherently scattered diffuse intensity, I_D. For Mo $K\alpha$ no monitor was employed as the measurements took only two days. No Fe fluorescence could be detected.

After correction for background the measured intensity was transformed into electron units per atom I_{eu}/N. Because of the extreme depth of penetration of Mo $K\alpha$ in the polystyrene the scattering from it could not be obtained precisely. So I_0 was established as follows. 21 data points were measured with both Co and Mo radiation. I_D for Co $K\alpha$ was calculated and the common points were multiplied by $(f^2_{Fe})_{MoK\alpha}/(f^2_{Fe})_{CoK\alpha}$. A direct beam intensity, I_0, for Mo $K\alpha$ was

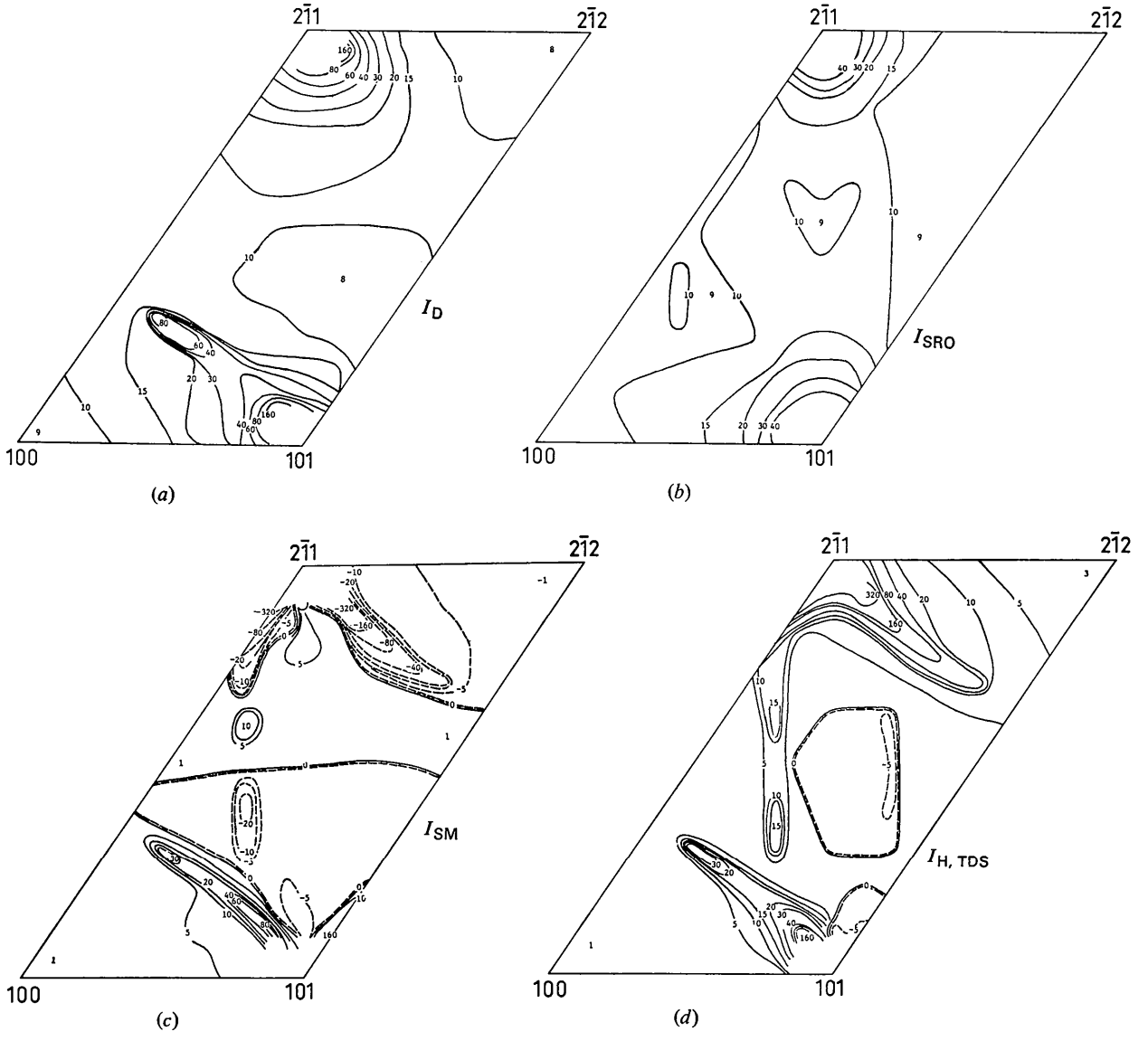

Fig. 3. Sections of the diffuse intensity (in electron units) through the explored volume parallel to $(\frac{1}{2},\frac{1}{2},0)$. (*a*) Total diffuse intensity, I_D; (*b*) Local-order intensity, I_{SRO}; (*c*) Size-effect modulation, I_{SM}; (*d*) Huang plus TDS intensity, $I_{H,TDS}$.

then chosen so that agreement to within 10% was obtained between I_D calculated from the Mo $K\alpha$ data and the transformed I_D from the Co $K\alpha$ data. The direct beam intensity so chosen was $0{\cdot}47\times10^8$ cps. [The choice of the f^2_{Fe} ratio as a multiplying factor rather than the ratio $(f_{Fe}-f_{Mo})^2$ (the term for I_{SRO}) is justified by the result of the separation procedure for these data points. $I_{H,TDS}$ makes up about 60% of the total diffuse intensity for the 21 data points and it depends on f^2_{Fe} (see Appendix II).]

Then

$$\frac{I_{eu}}{N}=\frac{2\text{ atomic weight}\times(\mu/\varrho)}{N_A\times p}\times\left(\frac{m^2c^4}{e^4}\right)\times\frac{R^2}{A}\times\frac{I}{I_0},\quad(28)$$

where N_A is Avogadro's Number, p is the polarization factor, R is the distance between the receiving slit and the sample, A, is the receiving slit area and I and I_0 are the measured intensity and the direct beam intensity, respectively. The mass absorption coefficient $(\mu/\varrho)=36{\cdot}5$ was taken from Heinrich (1966). The dif-

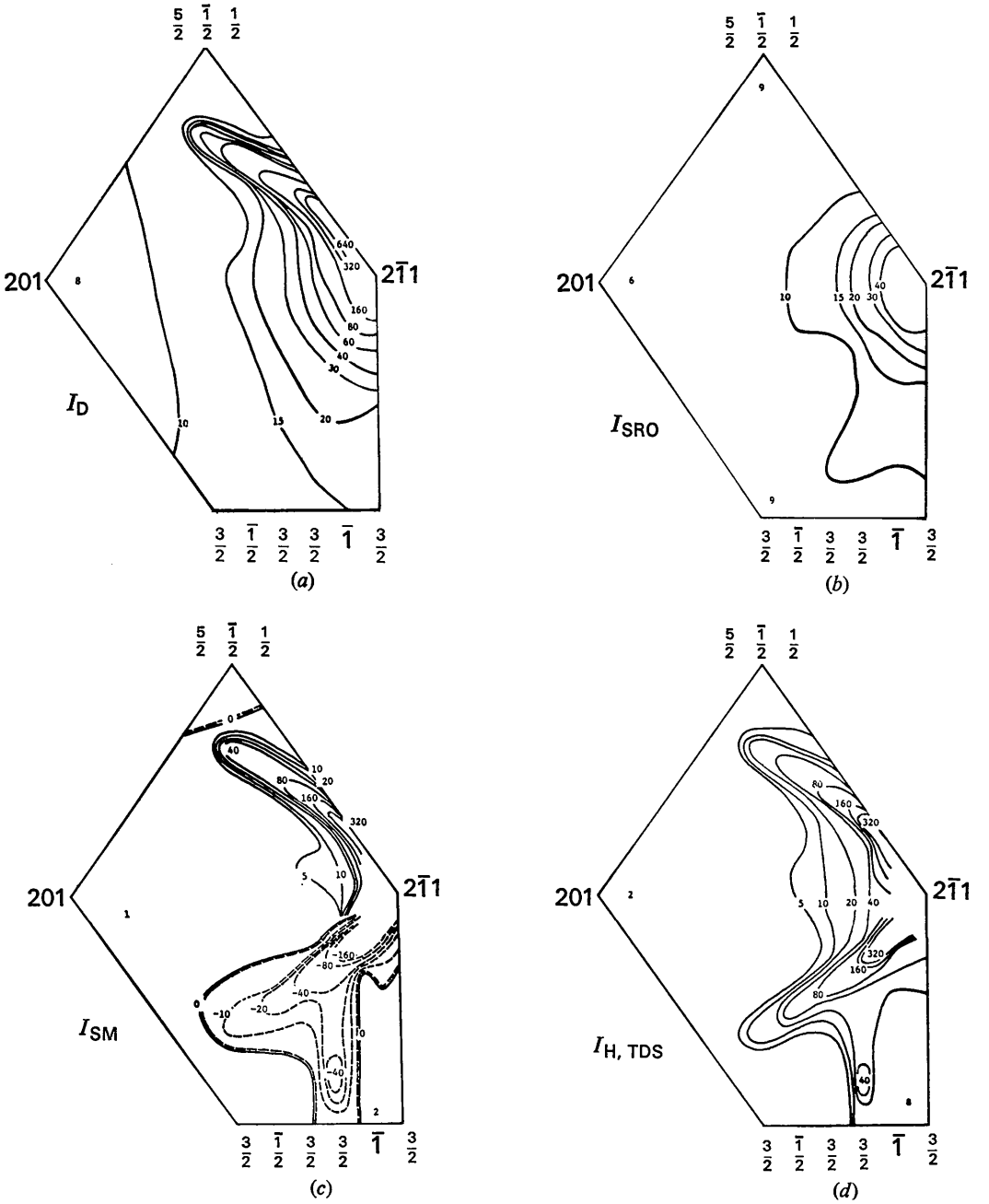

Fig. 4. Sections of the diffuse intensity (in electron units) through the explored volume parallel to $(\frac{1}{2},0,\frac{1}{2})$. (*a*) Total diffuse intensity, I_D; (*b*) Local-order intensity, I_{SRO}; (*c*) Size-effect modulation, I_{SM}; (*d*) Huang plus TDS intensity, $I_{H,TDS}$.

fuse intensity, I_D, was obtained from I_{eu}/N after subtraction of the Compton scattering taken from *International Tables for X-ray Crystallography* (1962).

I_D obtained with Mo $K\alpha$ was multiplied by $(f_{Fe})^2_{CoK\alpha}/(f_{Fe})^2_{MoK\alpha}$ so that all data was referred to the Co wavelength.

4. Results and discussion

Preliminary runs indicated that the diffuse intensity had its maximum at the fundamental peaks (101), (2$\bar{1}$1) and (301) indicating that there was clustering or at least no short-range order, for the intensity near the Bragg peaks could be only the Huang peak plus TDS. (It was for this reason that data points were concentrated near peaks.) Streaks of high intensity extend about 0·35 *h*-units from the peaks (101) and (2$\bar{1}$1) in approximately the [3 $\bar{3}$ $\bar{5}$] and [3 5 $\bar{3}$] directions respectively. Figs. 3(*a*) and 4(*a*) show two sections through the explored volume where the streaks are evident.

To carry out the three-dimensional Fourier analysis of I^0_{SRO} for α_l's it is necessary to extrapolate under the Bragg peaks. This extrapolation is not crucial however, Gragg (1970). I^0_{SRO} had also to be interpolated in areas far away from the peak to fill out all the 506 grid points in the minimum repeat volume for I^0_{SRO}. Knowing I^0_{SRO} in its repeat volume it can be generated throughout reciprocal space, particularly in a cube with its corners at (000), (100), (0$\bar{1}$0), (1$\bar{0}$0), (001), (101), (0$\bar{1}$1) and (1$\bar{1}$1). Three-dimensional Fourier analysis was performed in this cube to get the SRO parameters, and they are given in Table 1, column 1. Column 2 contains the values after subtracting the indicated constant background to make $\alpha_0=1$, as it should be theoretically. To further illustrate that the extrapolation under Bragg peaks is not important, in the last column are the changes in α_l, increasing the value of I^0_{SRO} at such peaks 16%.

To study the influence of errors in measurements due to counting statistics and to small errors in the angular settings a ± 5% relative random error was added to the measured intensity. This resulted in a ± 5% error in I_{SRO} and the resulting error in α_l was less than ± 0·0005. This error is even less than the change in α_l due to extrapolation (Table 1, column 5); therefore it is thought that α_l is accurate to the second decimal place.

The values corrected for the variation in scattering factors over the volume are in column 3. The value of α_0, 1·11 is the best yet reported. The constant subtraction needed to bring the value of α_0 to unity after this correction, 0·24 cps, is about 2·5% of a typical data point, and it is not unreasonable that some parasitic scattering of this order of magnitude was missed. The values of α's in this case are given in column 4.

Knowing I^0_{SRO}, Q_x, R_x and S_{yz} in the explored volume of reciprocal space I_{SRO}, I_{SM} and $I_{H,TDS}$ can be calculated separately from equation (22). They are plotted in the same two sections as their sum I_D [see Figs. 3(*b*), (*c*),(*d*) and 4(*b*), (*c*), (*d*)]. Note that most of the 'satellite' intensity seen in Figs. 3(*a*) and 4(*a*) is due to size modulation and Huang+thermal diffuse scattering. Outside the satellites and far from the Bragg peak I_{SRO} constitutes about 75% of I_D. Close to the peaks it is a smaller fraction, the smaller the higher the 2θ value of the peak.

To examine the local atomic arrangements corresponding to the order parameters, the computer program developed by Gehlen & Cohen (1965) and extended by Gragg (1970) to include up to 108,000 atoms was run with α_1, α_2 and α_3 given in Table 1. The program starts with any distribution of *A* and *B* atoms of a given composition (random in this case) and exchanges the atoms. After each exchange the specified α_1 for the distribution are calculated and when these values deviate less than a certain preset amount from the measured α_l (2% in this case) the program lists the final atomic distribution. The values for other

Table 1. *Warren local-order parameters* α_l *for* Fe–3·9 *at.% Mo*

Coordination shell	*lmn*	1 uncorrected	2 uncorrected 0·46 cps removed	3 corrected	4 corrected 0·24 cps removed	Change in α_l peak increased 16%
0	000	1·216	1·000	1·112	1·000	0·004
1	111	0·129	0·125	0·099	0·097	0·004
2	200	0·065	0·064	0·043	0·043	0·004
3	220	0·052	0·053	0·042	0·042	0·004
4	311	0·036	0·036	0·027	0·027	0·003
5	222	0·041	0·040	0·033	0·032	0·003
6	400	0·036	0·036	0·036	0·035	0·003
7	331	0·019	0·019	0·015	0·016	0·003
8	420	0·017	0·017	0·013	0·013	0·003
9	422	0·010	0·010	0·006	0·006	0·003
10′	511	0·012	0·012	0·010	0·010	0·002
10″	333	0·020	0·020	0·019	0·019	0·002
11	440	0·001	0·010	−0·001	−0·001	0·002
12	531	0·004	0·004	0·003	0·003	0·002

In column 1 are given α_l's calculated from I^0_{SRO}, in column 2 the same α_l's adjusted to $\alpha_0 \equiv 1$ by removing 0·46 cps from the measured data (5·0% of a typical point), in column 3 are given α_l's corrected for the variation of *f*'s in *Q*, *R* and *S* with $\sin\theta/\lambda$, in column 4 the same α_l's adjusted to $\alpha_0 \equiv 1$ by removing 0·24 cps (2·5% of a typical data point) and in column 5 the increase in α_l's when the peak value for I^0_{SRO} is increased. Although not reproduced here, the α_l's start to oscillate around zero at $i=14$.

α's for the final distribution can also be calculated and compared with measured values.

We have employed four sets of α_1, α_2 and α_3; the ones from column 1, 3 and 4 in Table 1 and a random set, *i.e.* $\alpha_1=\alpha_2=\alpha_3=0$. α_4, α_5 and α_6 were calculated to compare with experimental values. The model was 16,000 atoms ($20\times20\times20$ unit cells). In addition one run was carried out with α_1, α_2 and α_5, α_3 being calculated for comparison with the measured value. The measured and calculated α's for these cases are given in Table 2. The calculated α's are all smaller than the measured ones, the difference being approximately the same in all cases.

For a detailed analysis of the atomic distribution we have regarded two Mo atoms as a pair if they are first, second or third nearest neighbors. We have then calculated how many atoms belong to pairs, triplets, quadruplets, *etc.* Fig. 5 shows how many Mo atoms belong to clusters below a certain size for the five cases studied. There is a marked difference between the random case, no. 4 in Table 2, and the other four cases. The difference is very small between no. 2 and 5. In case no. 1 more atoms are in larger clusters, as is expected, α_1, α_2 and α_3 being larger. The medians of the curves for cases 1 to 5 are 7, 6, 6, 2 and 4 Mo atoms respectively. The average cluster sizes, excluding single Mo atoms and pairs are 7·9, 7·1, 7·6, 4·5 and 6·5 respectively.

A further study has been made of the clusters of case no. 3. Of the 29 clusters with two atoms, 9 were first, 7 were second and 13 third nearest neighbors. Of the 13 triplets only 4 had the most compact shape of two first nearest neighbor bonds and one second nearest neighbor. All clusters were rather open. Fig. 6 gives projections along the three unit-cell edges of the largest cluster of 39 atoms. If a cluster is inscribed in a box with its edges parallel to the unit cell edges (see Fig. 6) an average Mo concentration can be calculated. In Table 3 the average Mo concentration for all clusters with more than 9 atoms is given for computer runs 1, 2 and 3 in Table 3. The Mo content is between 5·5 and 16 at.% which is 1·4 and 4·1 respectively times the average value of 3·86 at.%. The clusters are rather irregular and most of them have no particularly long or short direction. Thus, there is no tendency for disk formation as might have been expected from Hornbogen's (1961) observations.

Table 2. *Experimental α-values used to generate atomic configurations and α-values calculated from these*

Case number	1		2		3		4		5	
α_i	Exp	Calc	Exp	Calc	Exp	Calc	Exp	Calc	Exp	Calc
1	0·129		0·099		0·097		0·000		0·099	
2	0·065		0·043		0·043		0·000		0·043	
3	0·052		0·042		0·042		0·000		0·042	0·018
4	0·036	0·015	0·027	0·007	0·027	0·006	0·000		0·027	0·004
5	0·041	0·012	0·033	0·010	0·032	0·003	0·000		0·033	
6	0·037	0·013	0·036	0·006	0·035	0·001	0·000		0·036	−0·006

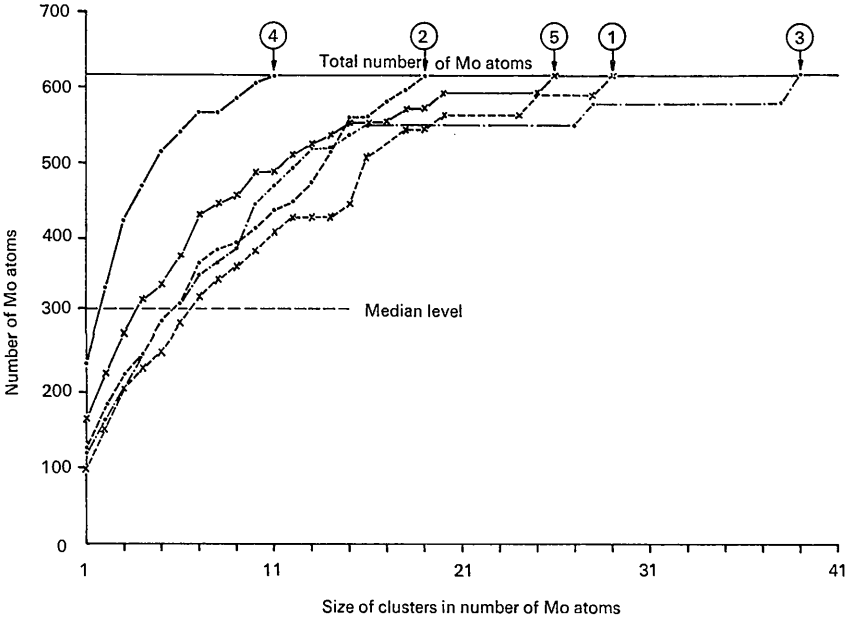

Fig. 5. The number of Mo atoms belonging to clusters below a size indicated on the abscissa. The circled numbers correspond to the cases defined in Table 2.

Table 3. *Average Mo concentration in boxes circumscribing clusters with* 10 *or more atoms*

Clusters size (number of Mo atoms)	Average Mo content (at.%)
10	9·7
11	11·9
12	9·3
13	11·1
14	11·5
15	7·7
16	9·1
17	13·1
18	7·3
19	6·0
20	16·0
25	6·2
28	8·8
29	3·5
39	4·8

In Appendix III, it is shown that Q_x for the chosen volume was also obtained in its minimum repeat volume in this study. As for I^0_{SRO} a three-dimensional Fourier analysis was carried out after extrapolation of Q_x under the Bragg peaks and interpolation in areas away from the peaks. The Fourier coefficients (γ^x_{lmn}) are defined in equation (6). For γ^x_{lmn} the following symmetry holds (Sparks & Borie, 1966)

$$\gamma^x_{lmn}=\gamma^x_{lnm}=-\gamma^x_{\bar{l}mn}=\gamma^x_{l\bar{m}n}=\gamma^x_{lm\bar{n}}\,.$$

However,

$$\gamma^x_{lmn}\neq\gamma^x_{mln} \quad \text{and} \quad \gamma^x_{lmn}\neq\gamma^x_{nml}\,.$$

Thus, contrary to α_{lmn}, γ^x_{lmn} is not the same for l, m, n belonging to a certain shell i.

γ^x_{lmn} is related to the x component of the atomic displacement δ through equations (6) and (9)–(11). If A designates Fe and B Mo then the term in equation (6) containing F^{FeFe}_{lmn} is dominant, because $x_{Fe}/x_{Mo}=25$ and we get:

$$\gamma^x_{lmn}\simeq 2\pi[f_{Fe}/(f_{Fe}-f_{Mo})]^2)(x_{Fe}/x_{Mo}+\alpha_{lmn})\langle x^{FeFe}_{lmn}\rangle. \quad (29)$$

The total displacement ($\bar{\delta}^{AA}_{lmn}$) is of more interest than the x component only. The y and z components can be calculated from γ^x because $\gamma^x_{nml}=\gamma^y_{lmn}=\gamma^z_{nml}$.

In Table 4 is given γ^x, the length of $\bar{\delta}^{AA}_{lmn}$ and its angle with the vector (l,m,n). The average displacements are quite small, the largest being about 2 pro mille of the smallest interatomic distance.

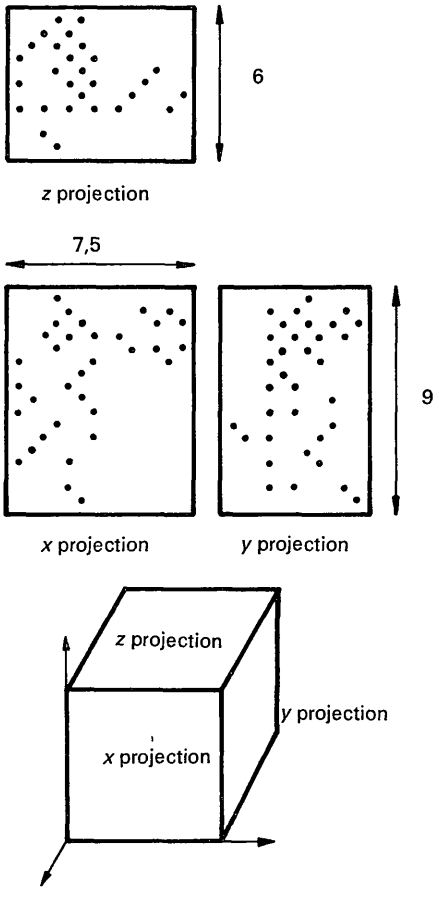

Fig. 6. Projections along unit-cell edges of a 39-atom cluster for case 3 in Table 3. Total volume: 405 unit cells. Average Mo content: 5 at.%.

Table 4. *The Fourier coefficients of* Q_x, *the average displacement between two* Fe *atoms* $\delta^{Fe\,Fe}$ *and the direction of this displacement,* φ, *relative to the interatomic vector* (l,m,n)

i	lmn	$\gamma^x{}_{lmn}$	$\lvert\delta_{lmn}{}^{FeFe}\rvert$	φ
1	111	−0·116	0·0022 Å	180°
2	200	−0·046	0·0005	180
2	020	0		
3		0·065	0·0010	0
4	311	0·043	0·0006	10
4	131	0·022		
5	222	0·003	0·00005	0
6	400	−0·057	0·0006	180
6	040	0		
7	331	−0·035	0·0007	156·1
7	133	−0·038		
8	420	−0·027		
8	240	−0·005	0·0003	165·0
8	024	0		

5. Conclusions

The necessary procedures have been developed and tested for separating the local-order intensity and size-effect modulation from the total diffuse intensity measured at only one temperature for a b.c.c. alloy. This procedure makes use of the symmetry of the contributions, as suggested by Sparks & Borie (1966) and Borie & Sparks (1971). The Warren local-order parameters α_i have been derived from the local-order intensity for Fe–3·86 at.% Mo and using α_1, α_2 and α_3 the atomic distribution has been generated by a computer. The

average cluster size was between 7 and 8 Mo atoms, the maximum size being around 40 Mo atoms. The shapes of these clusters were rather irregular without any pronounced short or long direction and the clusters had about twice the Mo concentration as the overall alloy composition. From an analysis of the size-effect modulation the average static displacement of an Fe atom from a lattice point was found to be quite small, of the order of 0·001 Å.

This work was supported by ARPA through Northwestern University's Materials Research Center. One of the authors (TE) was supported by the Swedish Natural Science Research Council. Thanks are also due to AB Atomenergi, Stockholm, Sweden for permission to use its computer facilities. Helpful discussions with Prof. J. Gragg (Carnegie-Mellon University) and the assistance of Mr H. Berg in making the computer runs on the atomic distributions is gratefully acknowledged.

APPENDIX I

The recovery of I^0_{SRO} in a b.c.c. crystal

It is sufficient to recover I^0_{SRO} in its minimum repeat volume as it is then known in the whole reciprocal lattice. One is free to chose many positions for this volume in the reciprocal lattice; essentially the volumes can be placed at any reciprocal lattice points. In this work, it was necessary to choose a position close to the origin as the radius of the limiting sphere for the Co radiation employed is fairly small, 1·6 h-units.

The total diffuse intensity, I_D, at the point h_1,h_2,h_3 is given by equation (22). Here (h_1,h_2,h_3) stands for all points within the chosen volume for I^0_{SRO} (see Fig. 1).

To separate I^0_{SRO} in (h_1,h_2,h_3) we must know Q_x, R_x and S_{yz} in (h_1,h_2,h_3), (h_2,h_1,h_3) and (h_3,h_2,h_1). (See equation 22). However, instead of the needed regions (h_2,h_1,h_3) and (h_3,h_2,h_1) we can take the regions $(-h_2, -h_1,h_3)$ and $(h_3,-h_1,-h_2)$, knowing from Sparks & Borie (1966) and Borie & Sparks (1971):

$$\left.\begin{aligned} Q_x(-h_2,-h_1,h_3) &= -Q_x(h_2,h_1,h_3)\\ R_x(-h_2,-h_1,h_3) &= R_x(h_2,h_1,h_3)\\ S_{yz}(h_3,-h_1,-h_2) &= S_{yz}(h_3,h_2,h_1)\\ S_{yz}(-h_1,-h_2,h_3) &= -S_{yz}(h_1,h_2,h_3)\end{aligned}\right\} \quad (A.1)$$

$$\left.\begin{aligned} Q_x(h_3,-h_1,-h_2) &= Q_x(h_3,h_2,h_1)\\ R_x(h_3,-h_1,-h_2) &= R_x(h_3,h_2,h_1)\\ S_{yz}(-h_2,-h_1,h_3) &= -S_{yz}(h_2,h_1,h_3)\\ S_{yz}(-h_1,h_3,-h_2) &= -S_{yz}(h_1,h_2,h_3)\end{aligned}\right\}. \quad (A.2)$$

Now, form the differences $\Delta_1^2 I_D(h_1,h_2,h_3)$ and $\Delta_1\Delta_2 I_D(h_1,h_2,h_3)$ according to equations (24) and (25).

$$\Delta_1^2 I_D(h_1,h_2,h_3) = 2R_x(h_1,h_2,h_3)\,, \quad (A.3)$$

$$\Delta_1\Delta_2 I_D(h_1,h_2,h_3) = S_{yz}(h_3,h_2,h_1)\,. \quad (A.4)$$

By permuting h_1,h_2 and h_3 in a proper way we also get

$$\Delta_1^2 I_D(-h_2,-h_1,h_3) = 2R_x(-h_2,-h_1,h_3) = 2R_x(h_2,h_1,h_3)\,, \quad (A.5)$$

$$\Delta_3\Delta_1 I_D(-h_2,-h_1,h_3) = S_{yz}(-h_1,h_2,-h_3) = -S_{yz}(h_1,h_2,h_3)\,. \quad (A.6)$$

[$\Delta_3\Delta_1$ is defined in analogy with $\Delta_1\Delta_2$, the difference being taken in the third and the first index instead of in the first and the second, see equation (A.17).]

$$\Delta_1^2 I_D(h_3,-h_1,-h_2) = 2R_x(h_3,h_2,h_1)\,, \quad (A.7)$$

$$\Delta_2\Delta_1 I_D(h_3,-h_1,-h_2) = S_{yz}(h_2,h_1,h_3)\,. \quad (A.8)$$

Thus, R_x and S_{yz} are recovered. To get Q_x form the difference $\Delta_1 I_D(h_1,h_2,h_3)$ according to equation (23) and in similar ways the differences $\Delta_1 I_D(-h_2,-h_1,h_3)$ and $\Delta_1 I_D(h_3,-h_1,-h_2)$.

$$\begin{aligned}\Delta_1 I_D(h_1,h_2,h_3) = {} & Q_x(h_1,h_2,h_3)\\ & +(2h_1-1)R_x(h_1,h_2,h_3)\\ & +h_2 S_{yz}(h_3,h_2,h_1)\\ & +h_3 S_{yz}(h_2,h_3,h_1)\,,\end{aligned} \quad (A.9)$$

$$\begin{aligned}\Delta_1 I_D(-h_2,-h_1,h_3) = {} & -Q_x(h_2,h_1,h_3)\\ & -(2h_2+1)R_x(h_2,h_1,h_3)\\ & -h_1 S_{yz}(h_3,h_2,h_1)\\ & -h_3 S_{yz}(h_1,h_2,h_3)\,,\end{aligned} \quad (A.10)$$

$$\begin{aligned}\Delta_1 I_D(h_3,-h_1,-h_2) = {} & Q_x(h_3,h_2,h_1)\\ & +(2h_3-1)R_x(h_3,h_2,h_1)\\ & +h_1 S_{yz}(h_2,h_1,h_3)\\ & +h_2 S_{yz}(h_1,h_2,h_3)\,.\end{aligned} \quad (A.11)$$

Inserting equation (A.3)–(A.8) into (A.9)–(A.11) gives Q_x. We now know all the quantities in equation (22) except $I^0_{SRO}(h_1,h_2,h_3)$ which can then be solved by taking the difference between the right and left hand sides of the equation. To form the intensity differences required in equations (A.3)–(A.11) we need to know the diffuse intensity in the following fifteen regions. (The factor $Nx_Ax_B(f_A-f_B)^2$ is omitted here for convenience.) The regions are underlined and numbered.

For:

$$\Delta_1 I_D(h_1,h_2,h_3) = \underline{I_D(h_1,h_2,h_3)}_{1} - \underline{I_D(h_1-1,h_2,h_3)}_{2}\,, \quad (A.12)$$

for:

$$\Delta_1^2 I_D(h_1,h_2,h_3) = \underline{I_D(h_1+1,h_2,h_3)}_{3} + I_D(h_1-1,h_2,h_3) - 2I_D(h_1,h_2,h_3)\,, \quad (A.13)$$

for:

$$\Delta_2\Delta_1 I_D(h_1,h_2,h_3) = \underline{I_D(h_1,h_2+1,h_3)}_{4} - \underline{I_D(h_1-1,h_2+1,h_3)}_{5} - I_D(h_1,h_2,h_3) + I_D(h_1-1,h_2,h_3)\,, \quad (A.14)$$

for:

$$\Delta_1 I_D(-h_2,-h_1,h_3) = \underline{I_D(-h_2,-h_1,h_3)}_{6} - \underline{I_D(-h_2-1,-h_1,h_3)}_{7}\,, \quad (A.15)$$

for:

$$\Delta I_{D1}^2(-h_2,-h_1,h_3) = \underline{I(-h_2+1,-h_1,h_3)}_{8} + I_D(-h_2-1,-h_1,h_3) - 2I_D(-h_2,-h_1,h_3)\,, \quad \text{(A.16)}$$

for:

$$\Delta_3\Delta_1 I_D(-h_2,-h_1,h_3) = I_D(-h_2,-h_1,h_3) - I_D(-h_2-1,-h_1,h_3) - \underline{I_D(-h_2,-h_1,h_3-1)}_{9} + \underline{I_D(-h_2-1,-h_1,h_3-1)}_{10}, \quad \text{(A.17)}$$

for:

$$\Delta_1 I_D(h_3,-h_1,-h_2) = \underline{I_D(h_3,-h_1,-h_2)}_{11} - \underline{I_D(h_3-1,-h_1,-h_2)}_{12}\,, \quad \text{(A.18)}$$

for:

$$\Delta_1^2 I_D(h_3,-h_1,-h_2) = \underline{I_D(h_3+1,-h_1,-h_2)}_{13} + I_D(h_3-1,-h_1,-h_2) - 2I_D(h_3,-h_1,-h_2)\,, \quad \text{(A.19)}$$

for:

$$\Delta_2\Delta_1 I_D(h_3,-h_1,-h_2) = \underline{I_D(h_3,-h_1+1,-h_1)}_{14} - \underline{I_D(h_3-1,-h_1+1,-h_2)}_{15} - I_D(h_3,-h_1,-h_2) + I_D(h_3-1,-h_1,-h_2). \quad \text{(A.20)}$$

By using the symmetry of I_D for a cubic crystal across the planes $h_1=0$, $h_2=0$, $h_3=0$, $h_2=-h_3$, $h_2=-h_1$, and $h_1=h_3$ we can reduce the number of regions to ten continuous regions. The numbers in the rectangles refer to the fifteen regions. In all cases the volume identified in Fig. 2 is the one in the set indicated by $I(j)$.

$$I(h_1,h_2,h_3)=I(-h_2,-h_1,h_3)=I(h_3,-h_1,-h_2)=I(1)\,, \quad \text{(A.21)}$$
[1] [6] [11]

$$I(h_1-1,h_2,h_3)=I(1-h_1,h_2,h_3)=I(2)\,, \quad \text{(A.22)}$$
[2]

$$I(h_1+1,h_2,h_3)=I(3)\,, \quad \text{(A.23)}$$
[3]

$$I(h_1,h_2+1,h_3)=I(h_1,-h_2-1,h_3) \quad [4]$$
$$=I(h_1,-h_3,h_2+1)=I(h_3,-h_1,h_2+1)$$
$$=I(h_2+1,-h_1,h_3)=I(5)\,, \quad \text{(A.24)}$$

$$I(h_1-1,h_2+1,h_3)=I(1-h_1,-h_2-1,h_3) \quad [5]$$
$$=I(1-h_1,-h_3,h_2+1)=I(4)\,, \quad \text{(A.25)}$$

$$I(-h_2,-h_1,h_3)=I(h_3,-h_1,-h_2)=I(1)\,, \quad \text{(A.26)}$$
[6] [11]

$$I(-h_2-1,-h_1,h_3)=I(h_2+1,-h_1,h_3)=I(5)\,, \quad \text{(A.27)}$$
[7]

$$I(-h_2+1,-h_1,h_3)=I(6)\,, \quad \text{(A.28)}$$
[8]

$$I(-h_2,-h_1,h_3-1)=I(1-h_3,-h_1,-h_2)=I(7)\,, \quad \text{(A.29)}$$
[9]

$$I(-h_2-1,-h_1,h_3-1)=I(h_2+1,-h_1,1-h_3)=I(8)\,, \quad \text{(A.30)}$$
[10]

$$I(h_3,-h_1,-h_2)=I(1)\,, \quad \text{(A.31)}$$
[11]

$$I(h_3-1,-h_1,-h_2)=I(1-h_3,-h_1,-h_2)=I(7)\,, \quad \text{(A.32)}$$
[12]

$$I(h_3+1,-h_1,-h_2)=I(9)\,, \quad \text{(A.33)}$$
[13]

$$I(h_2,-h_1+1,-h_2)=I(h_2,h_1-1,-h_2)=I(h_3,h_2,-h_1+1) \quad [14]$$
$$=I(h_1-1,h_2,h_3)=I(1-h_1,h_2,h_3)=I(2)\,, \quad \text{(A.34)}$$
[2]

$$I(h_3-1,-h_1+1,-h_2)=I(1-h_3,h_1-1,-h_2) \quad [15]$$
$$=I(1-h_3,h_2,-h_1+1)$$
$$=I(1-h_1,h_2,1-h_3)$$
$$=I(10)\,. \quad \text{(A.35)}$$

For a certain point (h_1,h_2,h_3) in the minimum repeat volume for I^0_{SRO} these expressions give the ten points in which the intensity has to be measured. Let us denote by $I(j)$ the diffuse intensity divided by $Nx_Ax_B(f_A-f_B)^2$ in volume j. The following set of equations has been used to derive I^0_{SRO} by combining equations (A.3)–(A.35).

$$R_x(h_1,h_2,h_3)=0{\cdot}5[I(3)+I(2)-2I(1)]\,, \quad \text{(A.36)}$$

$$R_x(h_2,h_1,h_3)=0{\cdot}5[I(6)+I(5)-2I(1)]\,, \quad \text{(A.37)}$$

$$R_x(h_3,h_2,h_1)\,0{\cdot}5[I(9)+I(7)-2I(1)]\,, \quad \text{(A.38)}$$

$$S_{yz}(h_3,h_1,h_2)=I(5)-I(4)-I(1)+I(2)\,, \quad \text{(A.39)}$$

$$S_{yz}(h_1,h_2,h_3)=I(7)-I(8)-I(1)+I(5)\,, \quad \text{(A.40)}$$

$$S_{yz}(h_2,h_3,h_1)=-I(2)+I(10)+I(1)-I(7)\,, \quad \text{(A.41)}$$

$$Q_x(h_1,h_2,h_3)=I(1)-I(2)+(2h_2+1)R_x(h_1,h_2,h_3) + h_3S_{yz}(h_3,h_1,h_2)-h_1S_{yz}(h_2,h_3,h_1)\,, \quad \text{(A.42)}$$

$$Q_x(h_2,h_1,h_3)=-I(1)+I(5)+(2h_3-1)R_x(h_2,h_1,h_3) + h_2S_{yz}(h_3,h_1,h_2)-h_1S_{yz}(h_1,h_2,h_3)\,, \quad \text{(A.43)}$$

$$Q_x(h_3,h_1,h_2)=I(1)-I(7)-(2h_1-1)R_x(h_3,h_2,h_1) + h_2S_{yz}(h_2,h_3,h_1)+h_3S_{yz}(h_1,h_2,h_3)\,, \quad \text{(A.44)}$$

$$I^0_{SRO}=I(1)-[-h_2Q_x(h_1,h_2,h_3)-h_3Q_x(h_2,h_1,h_3)+h_1Q_x(h_3,h_1,h_2)+h_2^2R_x(h_1,h_2,h_3)+h_3^2R_x(h_2,h_1,h_3)+h_1^2R_x(h_3,h_2,h_1)+h_2h_3S_{yz}(h_3,h_1,h_2)-h_3h_1S_{yz}(h_1,h_2,h_3)-h_1h_2S_{yz}(h_2,h_3,h_1)]\,. \quad (A.45)$$

APPENDIX II

Correction for the variation in scattering factor ratios in Q, R and S with sin θ/λ

Consider first the expression for the size-effect-modulation I_{SM}, given by equations (3), (6) and (9)–(11). The average displacement for any vector type (mn) must equal zero (Warren, Averbach & Roberts, 1951). Hence

$$x_A p^{AB}_{mn}(\underline{\delta}^{AB}_{mn}\underline{\delta})+x_B p^{BA}_{mn}(\underline{\delta}^{BA}_{mn})+x_A p^{AA}_{mn}(\underline{\delta}^{AA}_{mn})+x_B p^{BB}_{mn}(\underline{\delta}^{BB}_{mn})=0\,, \quad (B.1)$$

where p^{AB}_{mn} is the probability of finding a B atom at m when an A atom is at n. Sparks & Borie (1966) have shown that this condition simplifies the expression for γ^x_{mn}

$$\gamma^x_{lmn}=2\pi\left\{\frac{f_A}{(f_A-f_B)}\left(\frac{x_A}{x_B}+\alpha_{lmn}\right)\langle x^{AA}_{lmn}\rangle-\frac{f_B}{(f_A-f_B)}\left(\frac{x_B}{x_A}+\alpha_{lmn}\right)\langle x^{BB}_{lmn}\rangle\right\}\,. \quad (B.2)$$

Let A stand for Fe and B for Mo. Then in our case $x_A/x_B=25$ and the first term in equation (B.2) is dominant. Combining equation (13) and (B.2) we then get

$$(f_{Mo}-f_{Fe})^2Q_x=-f_{Fe}(f_{Fe}-f_{Mo})\times\sum_l\sum_m\sum_n 2\pi(x_{Fe}/x_{Mo}+\alpha_{lmn})\langle x^{FeFe}_{lmn}\rangle\times\sin 2\pi(h_1l+h_2m+h_3n)\,. \quad (B.3)$$

A function that is more independent of sin θ/λ than Q_x can be defined as

$$q_x=-(f_{Fe}-f_{Mo})/f_{Fe}\cdot Q_x\,. \quad (B.4)$$

Following a similar procedure for R_x and S_{yz} equations (14) and (15) can be written

$$(f_{Mo}-f_{Fe})^2R_x\simeq f^2_{Fe}\sum_l\sum_m\sum_n(-2\pi^2)(x_{Fe}/x_{Mo}+\alpha_{lmn})\times\langle(x^{FeFe}_{lmn})^2\rangle\cos 2\pi(h_1l+h_2m+h_3n)\,, \quad (B.5)$$

$$(f_{Mo}-f_{Fe})^2S_{yz}\simeq f^2_{Fe}\sum_l\sum_m\sum_n(-4\pi^2)(x_{Fe}/x_{Mo}+\alpha_{lmn})\times\langle y^{FeFe}_{lmn}z^{FeFe}_{lmn}\rangle\cos 2\pi(h_1l+h_2m+h_3n)\,. \quad (B.6)$$

Functions more independent of sin θ/λ than R_x and S_{yz} are

$$r_x=(f_{Mo}-f_{Fe})^2/f^2_{Fe}R_x\,, \quad (B.7)$$

$$s_{yz}=(f_{Mo}-f_{Fe})^2/f^2_{Fe}S_{yz}\,. \quad (B.8)$$

The transformation in equations (B.4), (B.7) and (B.8) is performed with values of f_{Mo} and f_{Fe} only for points in subvolume 1, see Fig. 2 after the initial separation. A modified diffuse intensity due to the modulation, I'_{SM}, and to thermal diffuse plus Huang scattering $I'_{H,TDS}$ can then be calculated in the entire measured volume according to a modified equation (22)

$$(I'_{SM}+I'_{H,TDS})/Nx_Ax_B=f_{Fe}(f_{Mo}-f_{Fe})[h_1q_x(h_1,h_2,h_3)+h_2q_x(h_2,h_1,h_3)+h_3q_x(h_3,h_2,h_1)]+f^2_{Fe}[h_1^2r_x(h_1,h_2,h_3)+h_2^2r_x(h_2,h_1,h_3)+h_3^2r_x(h_3,h_2,h_1)+h_1h_2s_{yz}(h_3,h_2,h_1)+h_2h_3s_{yz}(h_1,h_2,h_3)+h_3h_1s_{yz}(h_2,h_3,h_1)]\,. \quad (B.9)$$

The separation is performed again, and a small portion of the data appears as I_{SRO} (although there was none in the input), because the variation in scattering factor with sin θ/λ alters the symmetry of Q, R and S. This portion is the correction to be subtracted from I_{SRO} from the first separation. This data is then Fourier inverted to give a corrected set of α_i.

APPENDIX III

The derivation of Q_x in its minimum repeat volume

Q_x is defined by equation (13)

$$Q_x(h_1,h_2,h_3)=-\sum_l\sum_m\sum_n\gamma^x_{lmn}\sin 2\pi(h_1l+h_2m+h_3n)\,. \quad (13)$$

Let us consider another point (h'_1,h'_2,h'_3) in reciprocal lattice whose coordinates are

$$h'_1=\tfrac{1}{2}-h_1\,, \quad (C.1)$$

$$h'_2=-\tfrac{1}{2}-h_2\,, \quad (C.2)$$

$$h'_3=h_3\,. \quad (C.3)$$

We then get

$$\begin{aligned}Q_x(h'_1,h'_2,h'_3)&=-\sum_l\sum_m\sum_n\gamma^x_{lmn}\sin 2\pi[(\tfrac{1}{2}-h_1)l-(\tfrac{1}{2}+h_2)m+h_3n]\\&=-\sum_l\sum_m\sum_n\gamma^x_{lmn}\sin 2\pi[h_1(-l)+h_2(-m)+h_3n+\tfrac{1}{2}(l-m)]\,. \quad (C.4)\end{aligned}$$

For a b.c.c. lattice $(l-m)$ is even, therefore

$$\begin{aligned}Q_x(h'_1,h'_2,h'_3)&=-\sum_l\sum_m\sum_n\gamma^x_{lmn}\sin 2\pi[h_1(-l)+h_2(-m)+h_3n\\&=-\sum_l\sum_m\sum_n\gamma^x_{lmn}\sin 2\pi[h_1l+h_2m+h_3n]\,. \quad (C.5)\end{aligned}$$

The following symmetry relations hold for γ, (Sparks & Borie, 1966)

$$\gamma^x_{lmn}=-\gamma^{\underline{x}}_{\underline{l}mn}=-\gamma^{\underline{x}}_{l\underline{m}n}\,. \quad (C.6)$$

Inserting equation (C.6) into (C.5) gives

$$Q_x(h'_1,h'_2,h'_3)=-\sum_l\sum_m\sum_n(-\gamma^x_{lmn})\sin 2\pi(h_1l+h_2m+h_3n)=-Q_x(h_1,h_2,h_3)\,. \quad (C.7)$$

Let (h_1,h_2,h_3) represent the points in the minimum repeat volume for Q_x below the shaded plane in Fig. 1(*b*). Then (h_1',h_2',h_3') represents the points above the shaded plane; from equation (C.7) it is evident that when Q_x is known in the points (h_1,h_2,h_3) it is also known in the points (h_1',h_2',h_3'). Note that instead of the shaded plane in Fig. 1(*b*) any plane could be chosen containing a line which is parallel to the h_3 axis and goes through the point $(\frac{1}{4},\frac{1}{4},\frac{1}{4})$.

In Appendix I, $Q_x(h_1, h_2, h_3)$, $Q_x(h_2, h_1, h_3)$ and $Q_x(h_3,h_1,h_2)$ were derived, where (h_1,h_2,h_3) represents the points within the basic tetrahedron in Fig. 1(*a*). Due to the symmetries of Q_x (Sparks & Borie, 1966) we have

$$Q_x(-h_2,-h_1,h_3)=-Q_x(h_2,h_1,h_3)\,, \qquad \text{(C.8)}$$

and from the same type of reasoning as above we get

$$Q_x[(\tfrac{1}{2}-h_3),h_2,(\tfrac{1}{2}-h_1)]=-Q_x(h_3,h_2,h_1)\,.$$

The points (h_1,h_2,h_3), $(-h_2,-h_1,h_3)$ and $|(\frac{1}{2}-h_3),h_2,(\frac{1}{2}-h_1)|$ together fill out the part of the minimum repeat volume for Q_x below the shaded plane in Fig. 1 (b). [This can easily be checked by inserting the values for h_1,h_2,h_3 of the basic tetrahedron in Fig. 1(*a*)]. Thus, Q_x is known in its whole minimum repeat volume. The same type of reasoning leads to the conclusion that also R_x and S_{yz} are known in their minimum repeat volumes.

We thank Professor J. E. Gragg, Jr for pointing out to us the additional symmetry for b.c.c. systems that allows this separation.

References

BATTERMAN, B., CHIPMAN, D. R. & DE MARCO, J. (1961). *Phys. Rev.* **122**, 68.

BORIE, B. & SPARKS, C. J. (1971). *Acta Cryst.* In the press.

COOPER, M. J. (1963). *Acta Cryst.* **16**, 1067.

CROMER, D. T. & WABER, J. T. (1965). *Acta Cryst.* **18**, 104.

GEHLEN, P. C. & COHEN, J. B. (1965). *Phys. Rev.* **139**, A844.

GRAGG, J. (1970). PhD thesis. Northwestern Univ., Evanston, Ellinois.

HANSEN, M. (1958). *The Constitution of Binary Alloys.* New York: McGraw-Hill.

HEINRICH, K. F. J. (1966). *The Electron Microprobe.* New York: John Wiley.

HORNBOGEN, E. (1961). *Z. Metallk.* **52**, 47. *J. Appl. Phys.* **32**, 135.

HORNBOGEN, E. (1966). *Arch. Eisenhüttenw.* **37**, 523.

International Tables for X-ray Crystallography. (1962). Vol. III. Birmingham: The Kynoch Press.

KETTUNEN, P. & FORSTÉN, Y. (1964). *Acta Pol. Scand.* ch. 27, 5.

MARCUS, H. L., FINE, M. E. & SCHWARTZ, L. H. (1967). *J. Appl. Phys.* **38**, 4750.

SCHWARTZ, L. H., MORRISON, L. A. & COHEN, J. B. (1963). *Advances in X-ray Analysis.* Vol. 7. New York: Plenum Press.

SINHA, A. K., BUCKLEY, R. A. & HUME-ROTHERY, W. (1967). *J. Iron St. Inst.* **205**, 191.

SPARKS, C. J. & BORIE, B. (1966). *Local Atomic Arrangements Studied by X-ray Diffraction.* New York: Gordon & Breach.

STRONG, S. L. & KAPLOW, R. (1967). *Acta Cryst.* **23**, 38.

WARREN, B. E., AVERBACH, B. L. & ROBERTS, B. W. (1951). *J. Appl. Phys.* **22**, 1493.

WARREN, B. E. & MOZZI, R. L. (1966). *Acta Cryst.* **21**, 459.

WOLFF, P. M. DE (1956). *Acta Cryst.* **9**, 682.

Acta Cryst. (1971). A**27**, 109

Dynamical Calculation of Electron Scattering by Plasmons in Aluminum

BY P. A. DOYLE*

School of Physics, University of Melbourne, Parkville, Victoria 3052, *Australia*

(*Received* 16 *July* 1969 *and in revised form* 9 *February* 1970)

Plasmon diffuse scattering (PDS) is calculated for Al(111) systematics using the multi-slice approach to dynamical electron scattering. It is found that PDS contributes strongly to Kikuchi bands, and to the decrease in the mean absorption coefficient which occurs when energy filtering is removed. Thickness fringes are found, which are similar to those for Bragg beams except at low thickness. The different behaviour in this region is explained. The effect of the (111) Kikuchi band on the variation of the path length for plasmon excitation with crystal tilt is considered in detail.

Introduction

The excitation of plasmons in crystals by fast incident electrons has been considered theoretically by several authors. An account of this work has been given by Pines (1964). However, dynamical interactions of the plasmon diffuse scattering (PDS) can be readily implied from experiments with the electron microscope, such as the PDS thickness fringes observed by Kamiya & Uyeda (1961).

These thickness fringes have been predicted by Fujimoto & Kainuma (1962, 1963), Fukuhara (1963), and Howie (1963), who treated the PDS as coherent. Hei-

* Present address: Aeronautical Research Laboratories, Box 4331, G. P. O., Melbourne 3001, Australia.